



**HAL**  
open science

## Investigation of the effect of water content on the mechanical behavior of track-bed materials under various coarse grain contents

Yu Su, Yu-Jun Cui, Jean-Claude Dupla, Jean Canou

► **To cite this version:**

Yu Su, Yu-Jun Cui, Jean-Claude Dupla, Jean Canou. Investigation of the effect of water content on the mechanical behavior of track-bed materials under various coarse grain contents. *Construction and Building Materials*, 2020, 263, pp.120206. 10.1016/j.conbuildmat.2020.120206 . hal-03045809

**HAL Id: hal-03045809**

**<https://enpc.hal.science/hal-03045809>**

Submitted on 22 Aug 2022

**HAL** is a multi-disciplinary open access archive for the deposit and dissemination of scientific research documents, whether they are published or not. The documents may come from teaching and research institutions in France or abroad, or from public or private research centers.

L'archive ouverte pluridisciplinaire **HAL**, est destinée au dépôt et à la diffusion de documents scientifiques de niveau recherche, publiés ou non, émanant des établissements d'enseignement et de recherche français ou étrangers, des laboratoires publics ou privés.



Distributed under a Creative Commons Attribution - NonCommercial 4.0 International License

1     **Investigation of the effect of water content on the mechanical behavior of**  
2                   **track-bed materials under various coarse grain contents**

3

4                   Yu Su, Yu-Jun Cui, Jean-Claude Dupla, Jean Canou

5

6                   Laboratoire Navier/CERMES, Ecole des Ponts ParisTech (ENPC), France

7

8

9

10

11

12

13

14     **Corresponding author**

15     Professor Yu-Jun Cui

16     Ecole des Ponts ParisTech, Laboratoire Navier/CERMES, 6 – 8 av. Blaise Pascal, Cité Descartes,  
17     Champs-sur-Marne, 77455 Marne – la – Vallée cedex 2, France

18     Tel.: +33 164153550

19     Fax: +33 164153562

20     E-mail address: [yu-jun.cui@enpc.fr](mailto:yu-jun.cui@enpc.fr)

## 21 Abstract

22 In the French conventional railway track, an interlayer was created naturally through the  
23 interpenetration of ballast and subgrade under the effect of long-term train loading. Field  
24 investigation showed that the proportion of ballast grains decreased over depth in the  
25 interlayer. Moreover, the water content of interlayer soils varies depending on the weather  
26 conditions, which can strongly affect the mechanical behavior of interlayer soil. In this study,  
27 the effect of water content on the mechanical behavior of interlayer soils under various coarse  
28 grain contents was investigated by monotonic triaxial tests. Three water contents ( $w = 17.6\%$ ,  
29  $10.6\%$ , and  $7.0\%$ ), five volumetric coarse grain contents ( $f_v = 0\%$ ,  $10\%$ ,  $20\%$ ,  $35\%$ , and  $45\%$ )  
30 and three confining pressures ( $\sigma_3 = 30$  kPa,  $60$  kPa and  $120$  kPa) were considered. Results  
31 showed that a decrease of  $w$  led to an increase of shear strength and soil stiffness due to the  
32 effect of suction, and to an increase of dilatancy due to the aggregation of fine soils. Moreover,  
33 the variations of maximum deviator stress  $q_{\max}$ , Young's modulus  $E_0$ , dilatancy angle  $\psi$  and  
34 friction angle  $\varphi$  with  $f_v$  followed a bi-linear pattern for the three  $\sigma_3$  values, defining a  
35 characteristic volumetric coarse grain content  $f_{v\text{-cha}}$  value for a given  $w$  value:  $f_{v\text{-cha}} \approx 25\%$ ,  $29\%$   
36 and  $33\%$  for  $w = 17.6\%$ ,  $10.6\%$  and  $7.0\%$ , respectively. The  $f_{v\text{-cha}}$  corresponded to the  
37 transition from a structure dominated by fine soils to a structure dominated by coarse grains.  
38 The increase of  $f_{v\text{-cha}}$  with the decrease of  $w$  could be attributed to the swelling and shrinkage  
39 of fines. While drying from optimum water content of fines  $w_{\text{opt-f}} = 13.7\%$  to a lower  $w_f$  value,  
40 more coarse grains were needed to constitute the global skeleton due to the increase of the  
41 global volume of macro-pores resulted from the shrinkage of fine soils. By contrast, while  
42 wetting from  $w_{\text{opt-f}} = 13.7\%$  to a higher  $w_f$  value, since the global volume of macro-pores

43 decreased due to the swelling of fine soils, less coarse grains were required to constitute the  
44 global skeleton.

45 **Keywords:** fabric/structure of soils; partial saturation; laboratory tests; compaction; shear  
46 strength

## 47 INTRODUCTION

48 Most French conventional railway track was constructed by putting the ballast layer on the  
49 subgrade soil directly. Due to the long-term train circulation, a layer namely interlayer was  
50 naturally formed in the substructure, mainly by the interpenetration of ballast and subgrade.  
51 Considering its high dry density ( $2.4 \text{ Mg /m}^3$ ) and high bearing capacity [1], the French  
52 railway company (SNCF) has decided to keep it as part of the substructure in the execution of  
53 the track renewal program [2].

54 Based on the field investigation, the content of ballast grains was found to decrease over  
55 depth [1]. Globally, the interlayer can be separated into two parts: the upper part dominated by  
56 ballast grains and the lower part dominated by fine soils. For the upper part, the effects of fine  
57 soils content and water content on the mechanical behavior were studied by Trinh et al. [3],  
58 Cui et al. [2], Duong et al. [4-6] and Lamas-Lopez et al. [7, 8] by performing monotonic and  
59 cyclic triaxial tests. In order to extend the study to the whole interlayer, Wang et al. [9-11] and  
60 Qi et al. [12] investigated the effect of coarse grain content  $f_v$  (volumetric ratio of coarse  
61 grains to total sample) on the mechanical behavior. Results revealed existence of a  
62 characteristic volumetric coarse grain content  $f_{v\text{-cha}}$ , below which the soil was characterised by  
63 a fine matrix with coarse grains floating in it, while beyond which the soil was characterised  
64 by a coarse grain skeleton. It is worth noting that in the previous studies, the effect of  $f_v$  on the  
65 mechanical behavior was investigated under constant water content conditions. This is  
66 obviously not the field condition where the water content varies depending on the weather  
67 conditions, resulting in changes in mechanical behavior. Therefore, from a practical point of

68 view, it appears essential to investigate the effect of water content on the mechanical behavior  
69 of interlayer soil.

70 There are several studies addressing the effect of coarse grain content on the mechanical  
71 behavior of soil. Seif El Dine et al. [13] worked on sandy matrix with  $f_v$  of gravels, showing  
72 an increase of shear strength with the increase of  $f_v$ . However, Vallejo [14] showed an  
73 opposite trend when the mass proportion of coarse particles was beyond 65% for a mixture of  
74 rock and sand. It is worth noting that the fines involved in their studies were cohesionless soils  
75 like sand and glass beads, which did not represent the natural fine soils in the interlayer. Wang  
76 et al. [9-11] studied the effect of  $f_v$  on the static and dynamic responses of interlayer soil, and  
77 identified a characteristic value  $f_{v\text{-cha}}$  that could be used to differentiate two distinct soil fabrics.  
78 Qi et al. [12] investigated the effect of the coefficient of uniformity  $C_u$  of coarse grains on the  
79 mechanical behavior of interlayer soils, and found that the decrease of  $C_u$  led to an increase of  
80  $f_{v\text{-cha}}$ . A few studies were undertaken to investigate the water content effect on the mechanical  
81 behavior of substructure soils in terms of shear strength, resilient modulus, etc. Trinh et al. [3]  
82 investigated the effect of water content on the mechanical behavior of fouled ballast at  
83 different water contents and found that the lower the water content, the higher the shear  
84 strength. Duong et al. [6] studied the effect of water content on the resilient modulus of the  
85 upper part interlayer soil by large-scale cyclic triaxial tests, and reported that the increase of  
86 water content gave rise to a decrease of resilient modulus. To the author's knowledge, there  
87 has been no work addressing the effect of water content on  $f_{v\text{-cha}}$ .

88 In this study, the effect of water content on the mechanical behavior of the interlayer soil  
89 at various  $f_v$  values was investigated by performing monotonic triaxial tests under different

90 confining pressures. Three water contents (17.6%, 10.6%, and 7.0%), five coarse grain  
91 contents (0%, 10%, 20%, 35%, and 45%) and three confining pressures (30 kPa, 60 kPa and  
92 120 kPa) were considered. The mechanical properties including Young's modulus  $E_0$ ,  
93 Poisson's ratio  $\nu$ , dilatancy angle  $\psi$ , friction angle  $\varphi$  and cohesion  $c$  were analyzed. The results  
94 obtained allowed the effect of water content on the characteristic volumetric coarse grain  
95 content  $f_{v\text{-cha}}$  to be clarified.

96

## 97 MATERIALS AND METHODS

### 98 *Materials and sample preparation*

99 Since it was difficult to obtain intact interlayer soil, the studied soil was reconstituted in the  
100 laboratory. For the fines, in order to simulate the grain size distribution of fine soils from  
101 'Senissiat site' (Fig. 1), nine different commercial soils including sand and clay were mixed,  
102 with the pre-determined proportions shown in Table 1. The liquid limit and plasticity index of  
103 the reconstituted fine soil were 32% and 20%, respectively defining the fine soil as CL  
104 according to the universal soil classification system (Fig. 2). A good agreement between real  
105 fine soil and reconstituted fine soil was observed in terms of grain size distribution (Fig. 1),  
106 liquid limit and plasticity index (Fig. 2). Standard Proctor compaction was performed  
107 following ASTM D698-12 [15] for the reconstituted fine soil (Fig. 3), allowing an optimum  
108 water content  $w_{\text{opt-f}} = 13.7\%$  and a maximum dry density  $\rho_{\text{dmax-f}} = 1.82 \text{ Mg/m}^3$  to be identified.

109 For the coarse grains, following the parallel similitude method adopted by Wang et al. [10]  
110 and Qi et al. [12], micro-ballast was prepared to represent the real ballast by using three  
111 granular materials G 4-10, HN 2-4 and G 10-20, as shown in Fig. 4. In order to quantify the

112 amount of micro-ballast in a sample, a parameter namely volumetric coarse grain content  $f_v$   
113 [9-13] was adopted:

$$114 \quad f_v = V_{in} / V_{total} \quad (1)$$

115 where  $V_{in}$  and  $V_{total}$  represent the coarse grain volume and the total sample volume,  
116 respectively. Note that the total sample volume  $V_{total}$  was composed of the coarse grain volume  
117  $V_{in}$  and the fine soil volume  $V_{fines}$ . The dry density of fine soil in all samples was controlled at  
118  $\rho_{dmax-f} = 1.82 \text{ Mg/m}^3$  (Table 2). At a given  $f_v$  value, the dry mass of coarse grain, the dry mass  
119 of fine soil and the water content contained in the fine soil can be calculated. Details about the  
120 calculation could be found in Wang et al. [10].

121 For the preparation of samples at target  $f_v$  and  $w_f$ , the fine soil was prepared at optimum  
122 water content  $w_{opt-f} = 13.7\%$ , then stored in a container for 24 h for moisture homogenization.  
123 The fine soil was then mixed with micro-ballast grains thoroughly to reach the target  $f_v$  value.  
124 After that, the soil mixture was dynamically compacted in three layers to reach the size of 100  
125 mm diameter and 200 mm height. Note that at a given compaction effort, the dry density of  
126 fine soils changes with the variation of coarse grain content  $f_v$ . Since the dry density of fine  
127 soil in all samples was controlled at  $\rho_{dmax-f} = 1.82 \text{ Mg/m}^3$ , the compaction efforts was higher  
128 for the samples at higher  $f_v$  values. As a result, higher  $\rho_d$  values were obtained for the samples  
129 with higher  $f_v$  values, as shown in Table 2.

130 After reaching the target  $f_v$  value, either a wetting or a drying process was adopted to  
131 obtain the target  $w_f$ :  $w_1 = 17.6\%$  on the wet side of optimum;  $w_2 = 10.6\%$  and  $w_3 = 7.0\%$  on the  
132 dry side of optimum. In the case of drying process, considering that a too fast drying would



133 lead to sample damage by fissuring, a milder drying method was performed: the sample was  
134 exposed to the air in the laboratory for 1 h each time, and then enveloped with plastic film for  
135 equilibration. The time of equilibration needed was determined by measurement of suction  
136 and water content in three positions: in the center,  $\frac{1}{2} r$  and  $r$ , with  $r$  being radius of the sample.  
137 The results obtained showed that 7 h was required for reaching reasonable equilibration in  
138 terms of suction and water content (Table 3). In the case of wetting process, 10 g water was  
139 sprayed on the sample each time prior to covering it with plastic film for equilibration. The  
140 same equilibration time of at least 7 h was adopted.

141 When wetting or drying to a target  $w_f$ , the volume of sample was measured by means of a  
142 caliper. The volume changes from initial water content  $w_{\text{opt-f}} = 13.7\%$  to different target  $w_f$   
143 values are presented in Fig. 5. It appears that at a given  $f_v$  value, an increase of water content  
144 from  $w_{\text{opt-f}} = 13.7\%$  to  $w_1 = 17.6\%$  led to sample swelling, while a decrease of water content  
145 from  $w_{\text{opt-f}} = 13.7\%$  to  $w_2 = 10.6\%$  or  $w_3 = 7.0\%$  led to sample shrinkage. Moreover, under a  
146 given water content, the sample exhibited lower swelling-shrinkage with higher  $f_v$  values,  
147 illustrating the sensitivity of fine soil to water content changes. The measured dry densities of  
148 samples after wetting or drying are shown in Table 2.

149

#### 150 *Monotonic triaxial tests*

151 The mechanical behavior of soil at five different  $f_v$  values (0%, 10%, 20%, 35%, and 45%)  
152 and three different  $w_f$  contents (17.6%, 10.6%, and 7.0%) was investigated by monotonic  
153 triaxial tests, under three different  $\sigma_3$  values (30 kPa, 60 kPa and 120 kPa). Note that all

154 samples were prepared to reach the target water contents ( $w_1 = 17.6\%$  on the wet side, or  $w_2 =$   
155  $10.6\%$  and  $w_3 = 7.0\%$  on the dry side) prior to starting the test. For the samples at  $w_1 = 17.6\%$   
156 ( $S_r = 100\%$ ), an overnight consolidation under the corresponding confining pressure was  
157 adopted prior to shearing, to ensure the dissipation of pore water pressure. On the contrary, for  
158 the samples at  $w_2 = 10.6\%$  ( $S_r = 60\%$ ) or  $w_3 = 7.0\%$  ( $S_r = 40\%$ ), after an application of  $\sigma_3$ , the  
159 sample was directly sheared, because only air was expected to be expelled. A shear rate as  
160 low as  $0.1\text{mm/min}$  was adopted for all tests. The tests ended when a peak deviator stress  
161 appeared or the axial strain  $\varepsilon_1$  reached  $15\%$  in case without occurrence of peak deviator stress.

162

## 163 EXPERIMENTAL RESULTS

### 164 *Variation of shear behavior with $f_v$*

165 The variations of deviator stress  $q$  and volumetric strain  $\varepsilon_v$  with axial strain  $\varepsilon_1$  for samples at  
166  $w_1 = 17.6\%$  and five different  $f_v$  values are depicted in Fig. 6. It can be observed from Figs.  
167 6a<sub>1</sub>-6a<sub>3</sub> that under a given confining pressure  $\sigma_3$  value, the maximum deviator stress  $q_{\max}$   
168 increased slowly with the increase of  $f_v$  for  $f_v \leq 20\%$ , while the increase of  $q_{\max}$  was more  
169 pronounced for  $f_v \geq 35\%$ . The similar phenomena can be observed for the case of  $w_2 = 10.6\%$   
170 and  $w_3 = 7.0\%$ .

171 In Fig. 6b<sub>1</sub>, pure contractancy behaviour was observed for samples at  $f_v \leq 20\%$ , while for  
172 samples at  $f_v \geq 35\%$ , a behavior of contractancy followed by dilatancy was identified.  
173 Moreover, the larger the  $f_v$  value, the more pronounced the dilatancy behaviour. This dilatancy

174 was however reduced by the increase of confining pressure: when  $\sigma_3$  was increased from 60  
175 kPa (Fig. 6b<sub>2</sub>) to 120 kPa (Fig. 6b<sub>3</sub>), the contractancy increased and the dilatancy decreased.

176

### 177 *Variation of maximum deviator stress $q_{max}$ with $w$*

178 Fig. 7 depicts the variations of  $q_{max}$  against  $f_v$  at different  $\sigma_3$  values for three different water  
179 contents. In the case of  $w_1 = 17.6\%$  (Fig. 7a), it appeared that under a given  $\sigma_3$  value, the  
180 variation of  $q_{max}$  followed a bi-linear pattern with two different slopes, which defined a  
181 characteristic volumetric coarse grain content  $f_{v-cha}$ . Moreover, similar  $f_{v-cha}$  values (around  
182 25%) could be identified for the three different  $\sigma_3$  values. Physically, the  $f_{v-cha}$  value  
183 distinguished two different soil fabrics: when  $f_v \leq f_{v-cha}$ , the soil fabric was governed by fine  
184 soil dominated structure, while when  $f_v \geq f_{v-cha}$  it was governed by coarse grain dominated  
185 structure, in agreement with the observations by Wang et al. [10] and Qi et al. [12].

186 The same phenomena were observed for the two other water contents:  $w_2 = 10.6\%$  (Fig.  
187 7b) and  $w_3 = 7.0\%$  (Fig. 7c). For each water content,  $q_{max}$  varies in a bi-linear fashion with  
188  $f_v$ , defining a  $f_{v-cha}$  value which is independent of the  $\sigma_3$  value. The values of  $f_{v-cha}$  were 29%  
189 and 33% for  $w_2 = 10.6\%$  and  $w_3 = 7.0\%$ , respectively. Comparison of the  $f_{v-cha}$  values at  
190 different water contents showed that  $f_{v-cha}$  increased with the decrease of water content.

191

### 192 *Variation of Young's modulus $E_0$ with $w$*

193 In this study, the Young's modulus  $E_0$ , was defined as the ratio of deviator stress to axial  
 194 strain from 0% to 1%. Fig. 8 shows the variations of  $E_0$  with  $f_v$  under different  $\sigma_3$  values for the  
 195 three water contents. The effect of  $w$  on Young's modulus  $E_0$  can be clearly observed: at a  
 196 given  $f_v$  and  $\sigma_3$ ,  $E_0$  increased with the decrease of water content. This was attributed to the  
 197 increase of suction with the decrease of water content. At a given water content, a bi-linear  
 198 fitting could be also applied to represent changes of  $E_0$  with  $f_v$  for all  $\sigma_3$  values. This also  
 199 defined a characteristic volumetric coarse grain content  $f_{v\text{-cha}}$ , which was independent of  $\sigma_3$ .  
 200 As far as the variation of  $f_{v\text{-cha}}$  with  $w$  was concerned, it appeared from Fig. 8 that  $f_{v\text{-cha}}$   
 201 increased with the decrease of  $w$ :  $f_{v\text{-cha}}$  was around 25% for  $w_1 = 17.6\%$  (Fig. 8a), 29% for  $w_2 =$   
 202 10.6% (Fig. 8b) and 33% for  $w_3 = 7\%$  (Fig. 8c), which agreed well with the previous  
 203 observation while studying the effect of water content on  $q_{max}$  in Fig. 7.

204

#### 205 *Variations of Poisson's ratio $\nu$ and dilatancy angle $\psi$ with $w$*

206 Based on the volumetric strain-axial strain curves, the Poisson's ratio  $\nu$  and the dilatancy  
 207 angle  $\psi$  were determined using respectively Eqs. (1) and (2) [16]:

$$208 \quad \nu = (1 - k_c)/2 \quad (1)$$

$$209 \quad \sin \psi = k_D / (-2 + k_D) \quad (2)$$

210 where  $k_c$  and  $k_D$  are the slopes of volumetric strain-axial strain curves in the contractancy  
 211 phase and dilatancy phase, respectively.

212 Fig. 9 depicts the variations of Poisson's ratio  $\nu$  versus  $f_v$  at different  $\sigma_3$  values for three  
213 water contents. At  $w_1 = 17.6\%$  (Fig. 9a),  $\nu$  was not significantly influenced by  $\sigma_3$  and  $f_v$ , with  
214 the values fluctuating around  $\nu = 0.36$ . The values of  $\nu$  at  $f_v \leq 20\%$  were slightly larger than  
215 those at  $f_v \geq 35\%$ . This was due to the transition of soil fabric from fine soils dominated  
216 structure to coarse grains dominated structure, which resulted in the increase of soil stiffness  
217 and the decrease of horizontal strain. Moreover, the difference of  $\nu$  between  $f_v \leq 20\%$  and  $f_v \geq$   
218  $35\%$  decreased with the decrease of water content. The average value of  $\nu$  was 0.21 at  $w_2 =$   
219  $10.6\%$  (Fig. 9b) and 0.19 at  $w_3 = 7.0\%$  (Fig. 9c). At  $w_3 = 7.0\%$ , the  $\nu$  remained almost  
220 unchanged with the increase of  $f_v$ . Overall, it appeared that the average value of  $\nu$  decreased  
221 with the decreasing water content, suggesting that the lateral strain was reduced by the  
222 increase of suction or decrease of water content.

223 The effect of  $w$  on the dilatancy angle  $\psi$  can be clearly observed in Fig. 10: under given  $f_v$   
224 and  $\sigma_3$  values, the  $\psi$  increased with the decrease of  $w$ . This could be attributed to the  
225 aggregation of fine soil induced by the increase of suction. Indeed, a lower water content  
226 would generate a higher suction. In that case, the fine soils behaved more like granular  
227 materials, exhibiting more dilatancy behavior, as shown by Cui and Delage [17] and Ng et al.  
228 [18].

229 As shown in Fig. 10a ( $w_1 = 17.6\%$ ), no dilatancy behavior was observed for  $f_v$  varying  
230 from 0% to 20% at all  $\sigma_3$  values, whereas an obvious dilatancy behaviour was observed for  $f_v =$   
231  $35\%$  at  $\sigma_3 = 30$  kPa and for  $f_v = 45\%$  at all  $\sigma_3$  values. In addition, in Fig. 10b and Fig. 10c, a  
232 distinct change of  $\psi$  was observed from  $f_v \leq 20\%$  to  $f_v \geq 35\%$ , defining a value of characteristic

233 volumetric coarse grain content  $f_{v\text{-cha}} \approx 29\%$  at  $w_2 = 10.6\%$  and  $f_{v\text{-cha}} \approx 33\%$  at  $w_3 = 7.0\%$ . This  
234 increase of  $f_{v\text{-cha}}$  with the decrease of water content was consistent with the observation of  
235 water effect on  $q_{max}$  and  $E_0$ .

236

### 237 *Variations of cohesion $c$ and friction angle $\varphi$ with $w$*

238 The values of cohesion  $c$  and friction angle  $\varphi$  were determined based on the peak deviator  
239 stress values. Fig.11 depicts the variation of cohesion  $c$  with  $w$ . It can be observed that at a  
240 given  $f_v$ , the cohesion  $c$  increased with the decrease of water content. This could be attributed  
241 to the effect of suction on the fine soil.

242 For the friction angle  $\varphi$ , Fig.12 shows that  $\varphi$  increased with the decrease of  $w$ . This  
243 confirmed the aggregation phenomenon with the decrease of  $w$  for the fine soils. The similar  
244 observation was made by Zhao et al. [19] while studying the shear strength of a mixture of  
245 sand, silt and gravel. Moreover, under a given  $w$ , a bi-linear pattern of increasing trend with  $f_v$   
246 was observed for  $\varphi$ . A value of  $f_{v\text{-cha}}$  could be thus identified for each water content:  $f_{v\text{-cha}} \approx$   
247  $25\%$ ,  $29\%$ ,  $33\%$  for  $w = 17.6\%$ ,  $10.6\%$ ,  $7.0\%$ , respectively, in agreement with the effects of  
248 water content on  $q_{max}$ ,  $E_0$  and  $\psi$ .

249

## 250 DISCUSSIONS

251 The test results showed that the value of  $f_{v\text{-cha}}$  increased with the decrease of water content, as  
252 shown in Table 4. Wang et al. [10] obtained a value of  $f_{v\text{-cha}}$  equal to  $27\%$  at the optimum

253 water content  $w_{\text{opt-f}} = 13.7\%$ , which came to confirm the observation made in this study.

254 As mentioned before, the  $f_{v\text{-cha}}$  corresponded to the transition of soil fabric: when  $f_v \leq f_{v\text{-cha}}$ ,  
255 the soil fabric was the fine soils dominated structure, while when  $f_v \geq f_{v\text{-cha}}$ , the soil fabric  
256 changed to the coarse grains dominated structure. In other words, the  $f_{v\text{-cha}}$  represented the  
257 minimum  $f_v$  value needed for forming a coarse grains dominated structure. When  $f_v \geq f_{v\text{-cha}}$ ,  
258 two categories of fine soils were expected, namely a first category of dense fine soils situated  
259 between coarse grains and a second category of loose fine soils situated in the macro-pores  
260 surrounded by coarse grains. The former contributed to the loading-bearing skeleton of coarse  
261 grains, whereas the latter contributed little, as concluded by de Frias Lopez [20] through  
262 discrete element analysis.

263 The variation of  $f_{v\text{-cha}}$  with  $w$  could be attributed to the swelling upon wetting and  
264 shrinkage upon drying of these two categories of fines. With the decrease of water content, the  
265 two categories of fine soils would shrink. The shrinkage of the first category of fines would  
266 lead to a decrease of macro-pores between coarse grains, while the shrinkage of the second  
267 category would lead to an increase of macro-pores surrounded by coarse grains. As the  
268 density was expected to be higher and the quantity was expected to be smaller for the first  
269 category of fines, the decrease of macro-pores volume due to the shrinkage of the first  
270 category of fines was expected to be much smaller than the increase of macro-pores volume  
271 due to the shrinkage of the second category of fines. This was supported by the observation  
272 from Zhang and Li [21] using mercury intrusion porosimetry, who studied the fine/coarse soil  
273 mixture and reported that the structure supported by coarse grains was stable, and thus the  
274 shrinkage of clayey soils gave rise to an increase of the volume of macro-pores surrounded by

275 coarse particles. The effect of shrinkage of fine soils was also observed by Fies et al. [22] for  
276 the ternary mixtures of sand, silt and clay soils. They reported that when the fine fraction  
277 contained larger than 25% clay content, the shrinkage of fine fraction gave rise to the  
278 formation of macro-pores among the coarse fraction. It is worth noting that in this study, 30%  
279 of clay content of Speswhite and Bentonite were shown in Table 1 for the fine fraction, which  
280 contributed to the formation of macro-pores in the coarse grain skeleton. Thus, with the  
281 increase of volume of macro-pores, more coarse grains were needed to constitute a global  
282 skeleton. This is characterized by the increase of  $f_{v\text{-cha}}$  value.

283

## 284 CONCLUSIONS

285 The effect of  $w$  on the mechanical behavior of interlayer soil at various  $f_v$  was investigated by  
286 monotonic triaxial tests. Three water contents ( $w = 17.6\%$ ,  $10.6\%$ , and  $7.0\%$ ), five volumetric  
287 coarse grain contents ( $f_v = 0\%$ ,  $10\%$ ,  $20\%$ ,  $35\%$  and  $45\%$ ) and three confining pressures ( $\sigma_3 =$   
288  $30$  kPa,  $60$  kPa and  $120$  kPa) were considered. The obtained results allowed the following  
289 conclusions to be drawn.

290 The decrease of water content led to an increase of the peak deviator stress  $q_{\max}$  and the  
291 Young's modulus  $E_0$ . This could be explained by the effect of suction with the decrease of  
292 water content. The Poisson's ratio  $\nu$  was found to decrease with the decrease of water content,  
293 because the horizontal deformation was reduced by the increase of suction. The dilatancy  
294 angle  $\psi$  and the friction angle  $\phi$  were found to increase with the decrease of water content.  
295 This was attributed to the aggregation of fine soils induced by the increase of suction,



296 enhancing the dilatancy behavior and the friction of soil. A larger cohesion  $c$  was observed at  
297 lower  $w$ , also due to the effect of suction in fine soils.

298 The variation of  $q_{\max}$ ,  $E_0$ ,  $\psi$ , and  $\varphi$  with  $f_v$  followed a bi-linear pattern, defining a same  
299 characteristic  $f_{v\text{-cha}}$  value for a given  $w$  value:  $f_{v\text{-cha}} \approx 25\%$ ,  $29\%$  and  $33\%$  for  $w = 17.6\%$ ,  $10.6\%$   
300 and  $7.0\%$ , respectively. The value of  $f_{v\text{-cha}} \approx 27\%$  at  $w_{\text{opt}} = 13.7\%$  reported by Wang et al.  
301 (2018a) came to support this observation. This was attributed to the swelling upon wetting and  
302 shrinkage upon drying of two categories of fine soils: a first category of dense fine soil  
303 situated between coarse grains and a second category of loose fine soil situated in the macro-  
304 pores surrounded by coarse grains. With the decrease of water content, the two categories of  
305 fine soils would shrink. Moreover, the shrinkage of the first category of fines would lead to a  
306 decrease of macro-pores between coarse grains, while the shrinkage of the second category  
307 would lead to an increase of macro-pores surrounded by coarse grains. As the decrease of  
308 macro-pores volume due to the shrinkage of the first category of fines was expected to be  
309 much smaller than the increase of macro-pores volume due to the shrinkage of the second  
310 category of fines, the global macro-pores volume was increasing with the decrease of water  
311 content. In that case, more coarse grains were needed to constitute a global skeleton, leading  
312 to an increase of  $f_{v\text{-cha}}$ .

313

#### 314 ACKNOWLEDGEMENTS

315 This work was supported by the Chinese Scholar Council (CSC) and Ecole des Ponts  
316 ParisTech.

317

318 REFERENCES

319 [1] V. N. Trinh, Comportement hydromécanique des matériaux constitutifs de plateformes  
320 ferroviaires anciennes. PhD Thesis, Ecole Nationale des Ponts et Chaussées, Université  
321 Paris-Est, 2011.

322 [2] Y.J. Cui, T.V. Duong, A.M. Tang, J.C. Dupla, N. Calon, A. Robinet, Investigation of the  
323 hydro-mechanical behaviour of fouled ballast, Journal of Zhejiang University Science A.  
324 14(4) (2013) 244-255.

325 [3] V.N. Trinh, A.M. Tang, Y.J. Cui, J.C. Dupla, J. Canou, N. Calon, L. Lambert, A. Robinet,  
326 O. Schoen, Mechanical characterisation of the fouled ballast in ancient railway track  
327 substructure by large-scale triaxial tests, Soils and foundations. 52(3) (2012) 511-523.

328 [4] T.V. Duong, A.M. Tang, Y.J. Cui, V.N. Trinh, J.C. Dupla, N. Calon, J. Canou, A. Robinet,  
329 Effects of fines and water contents on the mechanical behavior of interlayer soil in  
330 ancient railway sub-structure, Soils and foundations. 53(6) (2013) 868-878.

331 [5] T.V. Duong, Y.J. Cui, A.M. Tang, J.C. Dupla, J. Canou, N. Calon, A. Robinet,  
332 Investigating the mud pumping and interlayer creation phenomena in railway sub-  
333 structure, Engineering geology. 171 2014 45-58.

334 [6] T.V. Duong, Y.J. Cui, A.M. Tang, J.C. Dupla, J. Canou, N. Calon, A. Robinet, Effects of  
335 water and fines contents on the resilient modulus of the interlayer soil of railway  
336 substructure, Acta Geotechnica. 11(1) 2016 51-59.

337 [7] F. Lamas-Lopez, S.C. d'Aguiar, A. Robinet, Y.J. Cui, N. Calon, J. Canou, J.C. Dupla,  
338 A.M. Tang, In-situ investigation of the behaviour of a French conventional railway

339 platform, In Proceedings of the transportation research board 94th annual meeting.  
340 Washington, DC (2015) 15-1076.

341 [8] F. Lamas-lopez, Field and laboratory investigation on the dynamic behavior of  
342 conventional railway track-bed materials in the context of traffic upgrade. PhD Thesis,  
343 Ecole Nationale des Ponts et Chaussées, Université Paris-Est, 2016.

344 [9] H.L. Wang, Y.J. Cui, F. Lamas-Lopez, J.C. Dupla, J. Canou, N. Calon, G. Saussine, P.  
345 Aïmedieu, R.P. Chen, Effects of inclusion contents on resilient modulus and damping  
346 ratio of unsaturated track-bed materials, Canadian Geotechnical Journal. 54(12) (2017)  
347 1672-1681.

348 [10] H.L. Wang, Y.J. Cui, F. Lamas-Lopez, N. Calon, G. Saussine, J.C. Dupla, J. Canou, P.  
349 Aïmedieu, R.P. Chen, Investigation on the mechanical behavior of track-bed materials at  
350 various contents of coarse grains, Construction and Building Materials. 164 (2018) 228-  
351 237.

352 [11] H.L. Wang, Y.J. Cui, F. Lamas-Lopez, J.C. Dupla, J. Canou, N. Calon, G. Saussine, P.  
353 Aïmedieu, R.P. Chen, Permanent deformation of track-bed materials at various inclusion  
354 contents under large number of loading cycles, Journal of Geotechnical and  
355 Geoenvironmental Engineering. 144(8) (2018) 04018044.

356 [12] S. Qi, Y.J. Cui, R.P. Chen, H.L. Wang, F. Lamas-Lopez, P. Aïmedieu, J.C. Dupla, J.  
357 Canou, G. Saussine, Influence of grain size distribution of inclusions on the mechanical  
358 behaviours of track-bed materials, Géotechnique. (2019) 1-10.

- 359 [13] B. Seif El Dine, J. C. Dupla, R. Frank, J. Canou, Y. Kazan, Mechanical characterization  
360 of matrix coarse-grained soils with a large-sized triaxial device, Canadian Geotechnical  
361 Journal. 47(4) (2010) 425-438.
- 362 [14] L.E. Vallejo, Interpretation of the limits in shear strength in binary granular mixtures,  
363 Canadian Geotechnical Journal. 38(5) (2001) 1097-1104.
- 364 [15] ASTM D698-12. Standard test methods for laboratory compaction characteristics of soil  
365 using standard effort. ASTM International, West Conshohocken, Pa, 2012)
- 366 [16] P.A. Vermeer, R. De Borst, Non-associated plasticity for soils, concrete and rock.  
367 HERON, 29(3) (1984) 1-64.
- 368 [17] Y.J. Cui, P. Delage, Yielding and plastic behaviour of an unsaturated compacted silt,  
369 Géotechnique. 46(2) (1996) 291-311.
- 370 [18] C.W.W. Ng, S. Baghbanrezvan, H. Sadeghi, C. Zhou, F. Jafarzadeh, Effect of specimen  
371 preparation techniques on dynamic properties of unsaturated fine-grained soil at high  
372 suctions, Canadian Geotechnical Journal. 54(9) (2017) 1310-1319.
- 373 [19] H.F. Zhao, L.M. Zhang, D.G. Fredlund, Bimodal shear-strength behavior of unsaturated  
374 coarse-grained soils, Journal of geotechnical and geoenvironmental engineering. 139(12)  
375 (2013) 2070-2081.
- 376 [20] R. de Frias Lopez, J. Silfwerbrand, D. Jelagin, B. Birgisson, Force transmission and soil  
377 fabric of binary granular mixtures, Géotechnique. 66(7) (2016)578-583.
- 378 [21] L.M. Zhang, X. Li, Microporosity structure of coarse granular soils, Journal of  
379 Geotechnical and Geoenvironmental Engineering. 136(10) (2010)1425-1436.

380 [22] J.C. Fiès, N.D.E., Louvigny, A. Chanzy The role of stones in soil water retention,  
381 European Journal of Soil Science. 53(1) (2002) 95-104.

382 NOTATIONS

$c$	cohesion
$E_0$	initial Young's modulus
$f_v$	volumetric coarse grain content
$f_{v\text{-cha}}$	characteristic volumetric coarse grain content
$k_c$	slope of volume change curve in the contractancy phase
$k_d$	slope of volume change curve in the dilatancy phase
$\rho_d$	dry density of sample
$\rho_{d\text{max-f}}$	maximum dry density of fine soil
$q$	deviator stress
$q_{\text{max}}$	peak deviator stress
$w_{\text{opt-f}}$	optimum water content of fine soil
$w_f$	water content of fine soil
$\varepsilon_a$	axial strain
$\varepsilon_v$	volumetric strain
$\sigma_3$	confining pressure
$\varphi$	friction angle
$\nu$	Poisson's ratio
$\psi$	dilatancy angle

383

384

385 LIST OF TABLES

- Table 1. The constitution of fine soil
- Table 2. Experimental program
- Table 3. Suction and water content measured at different equilibration times for fine soils
- Table 4.  $f_{v\text{-cha}}$  values at different water contents

386

387 LIST OF FIGURES

- Fig. 1. Grain size distribution curves of fine soils (after Wang et al. [10])
- Fig. 2. Plasticity of fine soils (after Wang et al. [10])
- Fig. 3. Samples states with respect to the compaction curve
- Fig. 4. Grain size distribution curves of micro-ballast and ballast (after Wang et al. [10])
- Fig. 5. Volume change of samples at different  $f_v$  values for the three target water contents
- Fig. 6. Results from the tests at  $w_1=17.6\%$  and different  $f_v$  values under:  
(a<sub>1</sub>) - (b<sub>1</sub>)  $\sigma_3= 30$  kPa; (a<sub>2</sub>) - (b<sub>2</sub>)  $\sigma_3= 60$  kPa; (a<sub>3</sub>) - (b<sub>3</sub>)  $\sigma_3= 120$  kPa
- Fig. 7. Variations of peak deviator stress with  $f_v$  under different  $\sigma_3$  values for:  
(a)  $w_1 = 17.6\%$ ; (b)  $w_2 = 10.6\%$ ; (c)  $w_3 = 7.0\%$
- Fig. 8. Variations of initial Young's modulus with  $f_v$  under different  $\sigma_3$  values for:  
(a)  $w_1 = 17.6\%$ ; (b)  $w_2 = 10.6\%$ ; (c)  $w_3 = 7.0\%$
- Fig. 9. Variations of Poisson's ratio with  $f_v$  under different  $\sigma_3$  values for:  
(a)  $w_1 = 17.6\%$ ; (b)  $w_2 = 10.6\%$ ; (c)  $w_3 = 7.0\%$
- Fig. 10. Variations of dilatancy angle with  $f_v$  under different  $\sigma_3$  values for:  
(a)  $w_1 = 17.6\%$ ; (b)  $w_2 = 10.6\%$ ; (c)  $w_3 = 7.0\%$
- Fig. 11. Variations of cohesion with  $f_v$  under different water contents
- Fig. 12. Variations of friction angle with  $f_v$  under different water contents

388

389

Table 1. The constitution of fine soil

Soil	Mass proportion (%)	Grain size range (mm)
HN34	3.3	0.063 - 0.50
HN31	3.3	0.16 - 0.63
HN0.4-0.8	6.7	0.25 - 1
HN0.6-1.6	6.7	0.32 - 2
HN1-2.5	13.3	0.32 - 3.20
C4	16.7	0.0009 - 0.50
C10	20	0.0009 - 0.25
Speswhite	23.3	0.0003 - 0.01
Bentonite	6.7	0.001 - 0.01

390

391



Table 2. Experimental program

$f_v$ (%)	Initial water content $w_{opt-f}$ (%)	Target $w_f$ (%)	Target $S_r$ (%)	Target $\rho_{dmax-f}$ (Mg/m <sup>3</sup> )	Target $\rho_d$ (Mg/m <sup>3</sup> )	Measured $\rho_d$ (Mg/m <sup>3</sup> )	Confining pressure $\sigma_3$ (kPa)		
0		17.6	100		1.82	1.80	30	60	120
		10.6	60			1.85	30	60	120
		7.0	40			1.86	30	60	120
10		17.6	100		1.91	1.88	30	60	120
		10.6	60			1.93	30	60	120
		7.0	40			1.94	30	60	120
20	13.7	17.6	100	1.82	1.99	1.97	30	60	120
		10.6	60			2.01	30	60	120
		7.0	40			2.03	30	60	120
35		17.6	100		2.12	2.11	30	60	120
		10.6	60			2.13	30	60	120
		7.0	40			2.13	30	60	120
45		17.6	100		2.21	2.20	30	60	120
		10.6	60			2.22	30	60	120
		7.0	40			2.23	30	60	120

Note:  $f_v$  represents the ratio of volumetric inclusion content to the total volume of the sample

[10].  $w_{opt-f}$ ,  $w_f$ ,  $S_r$  and  $\rho_{dmax-f}$  represent the optimum water content, the water content, the degree of saturation and the maximum dry density of fine soils, respectively.  $\rho_d$  represents the dry density of soil mixture sample. Measured  $\rho_d$  represents the dry density of soil mixture sample after wetting or drying from compaction water content  $w_{opt-f}$  to target  $w_f$ .

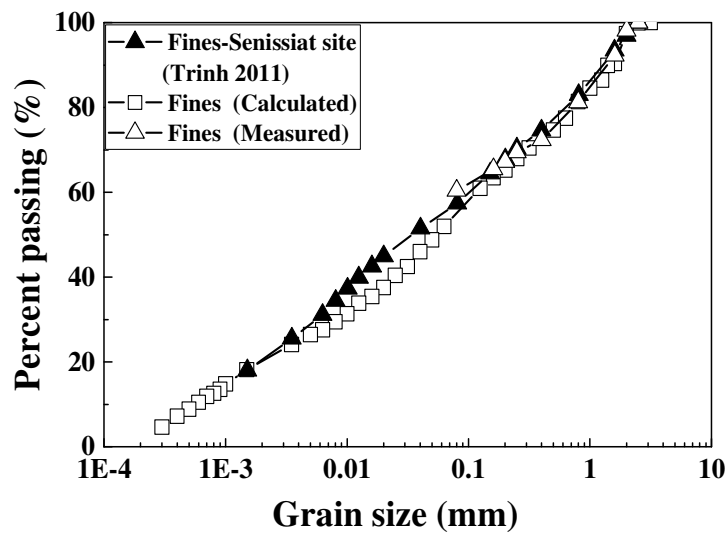
Table 3. Suction and water content measured at different equilibration times for fine soils

Position	Suction (MPa)	Water content (%)	Suction (MPa)	Water content (%)
	After 6h		After 7h	
center	0.33	12.7	0.32	12.9
1/2 r	0.24	13.5	0.35	12.8
r	0.46	13.7	0.33	13.1

Table 4.  $f_{v\text{-cha}}$  values at different water contents

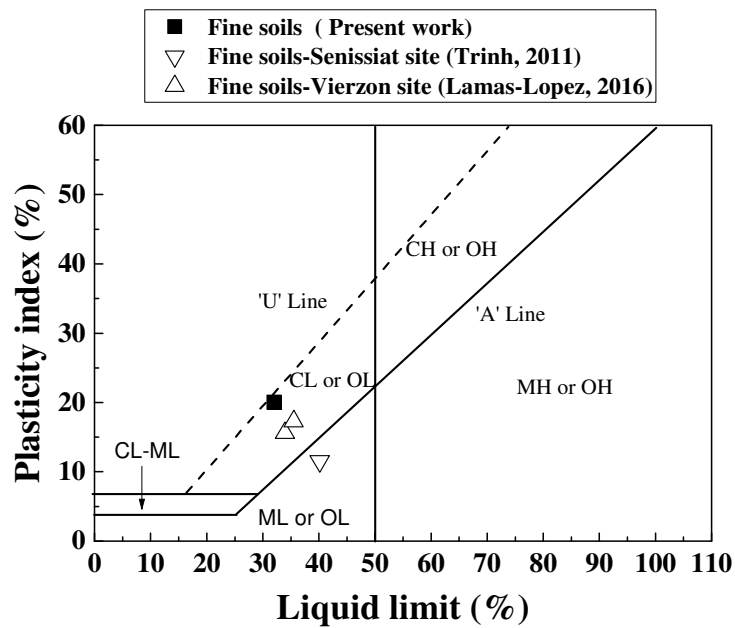
$w$ (%)	17.6	13.7	10.6	7.0
$f_{v\text{-cha}}$ (%)	25	27	29	33

Note:  $f_{v\text{-cha}} \approx 27\%$  corresponding to  $w = 13.7\%$  was obtained by Wang et al. [10]



394

Fig. 1. Grain size distribution curves of fine soils (after Wang et al. [10])



395

Fig. 2. Plasticity of fine soils (after Wang et al. [10])

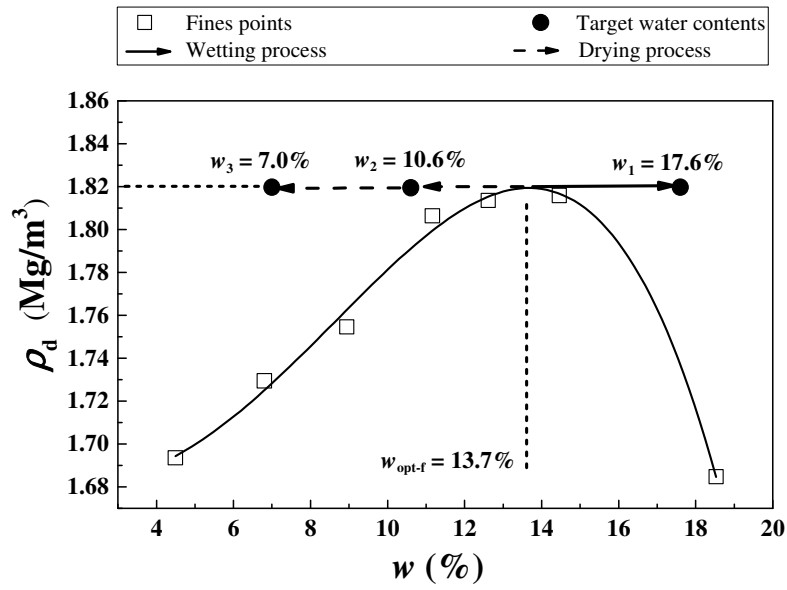


Fig. 3. Samples states with respect to the compaction curve

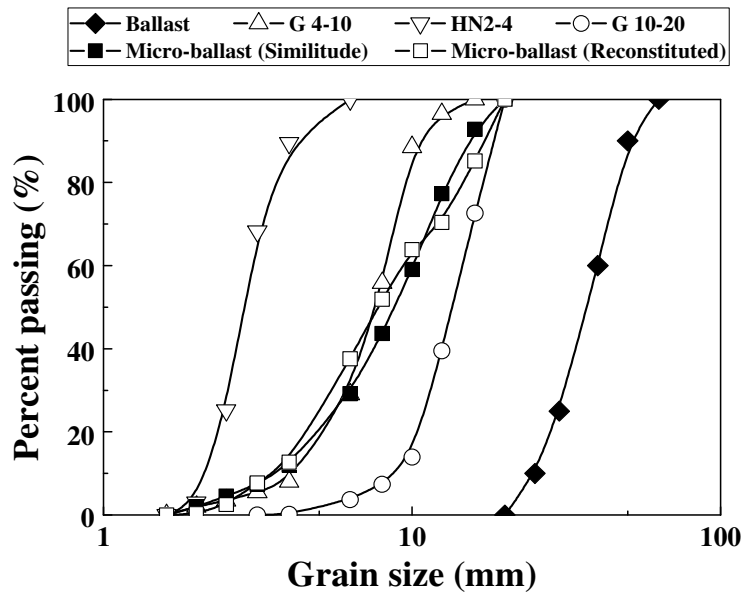
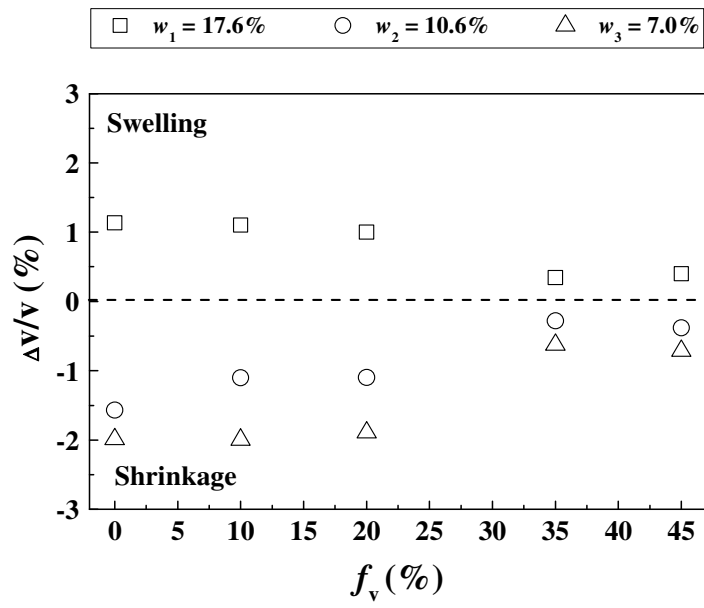


Fig. 4. Grain size distribution curves of micro-ballast and ballast (after Wang et al. [10])



397

398 Fig. 5. Volume change of samples at different  $f_v$  values for the three target water contents

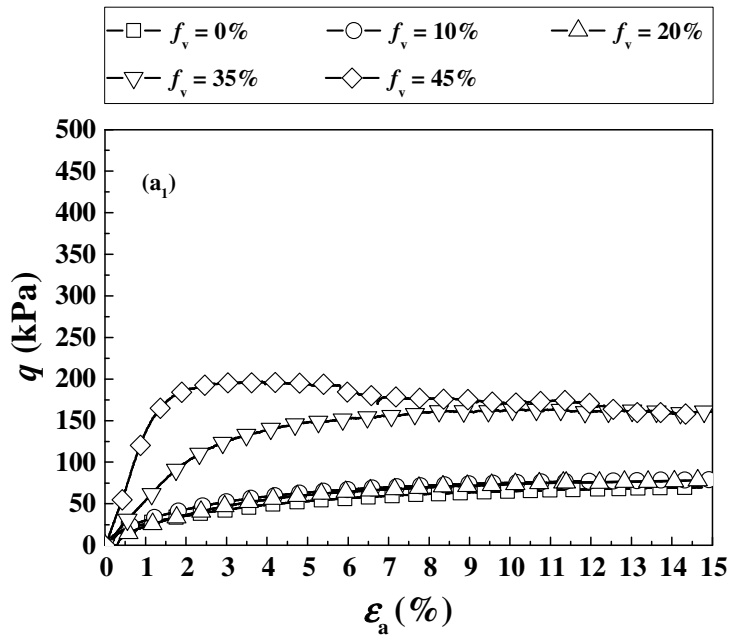
399

400

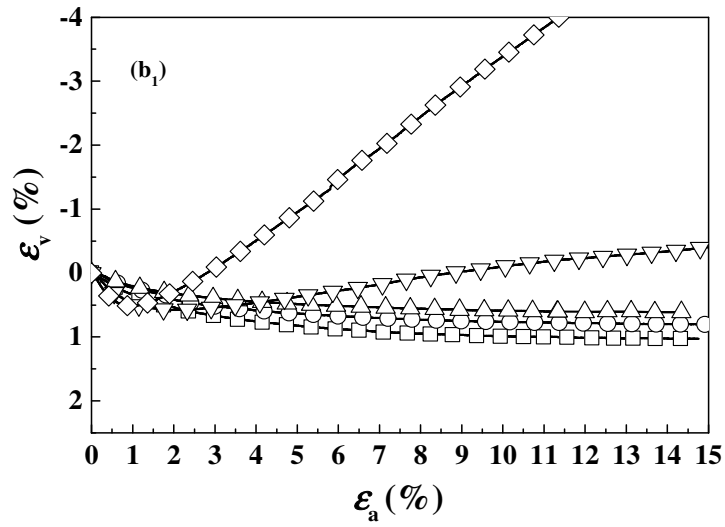
401

402

403



404



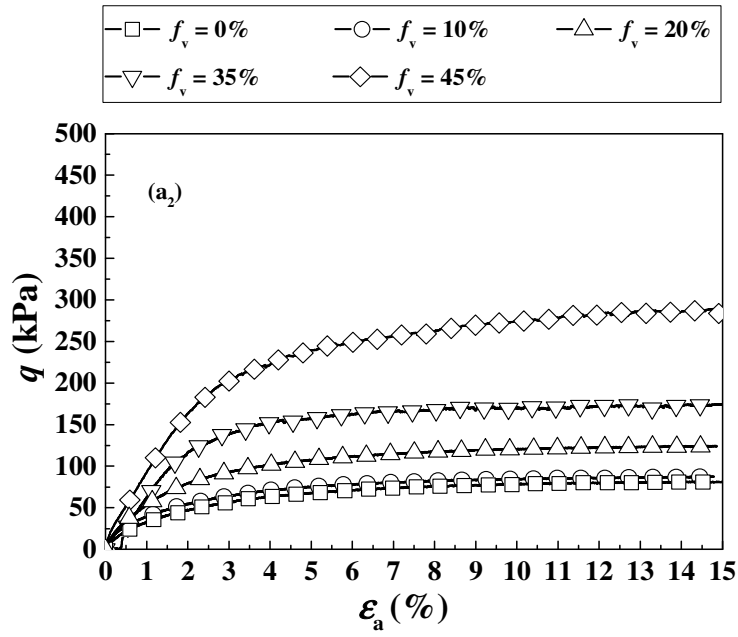
405

406

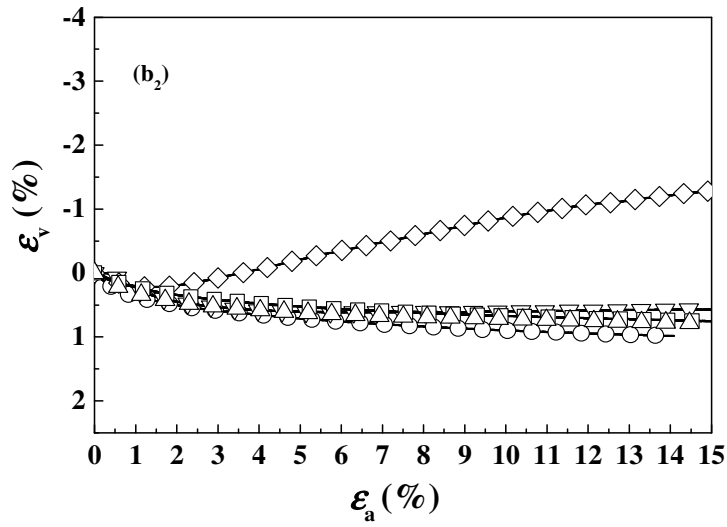
407

408

409



410



411

412

413

414

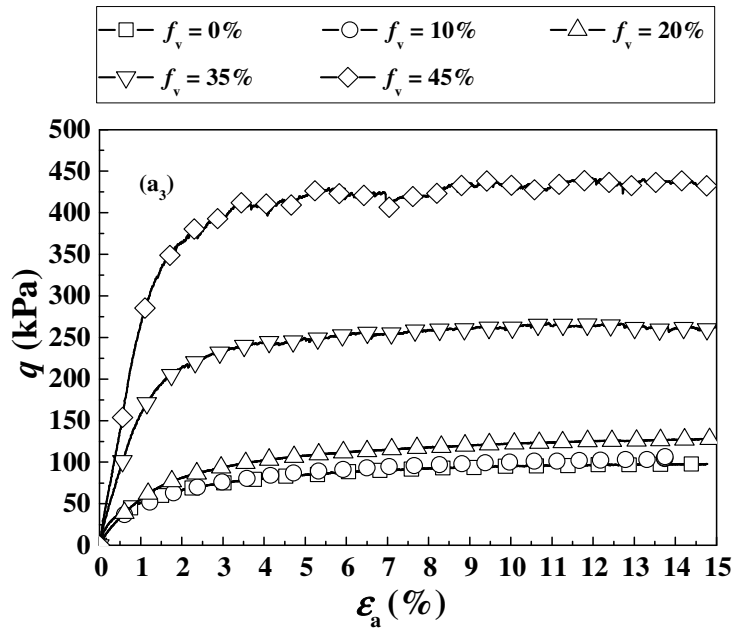
415

416

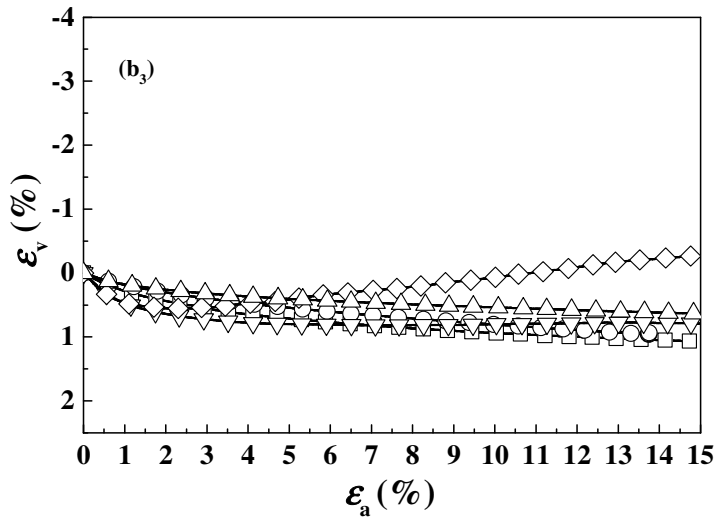
417

418

419



420



421

422

423

Fig. 6. Results from the tests at  $w_1=17.6\%$  and different  $f_v$  values under:

424

(a<sub>1</sub>) - (b<sub>1</sub>)  $\sigma_3 = 30$  kPa; (a<sub>2</sub>) - (b<sub>2</sub>)  $\sigma_3 = 60$  kPa; (a<sub>3</sub>) - (b<sub>3</sub>)  $\sigma_3 = 120$  kPa

425

426

427

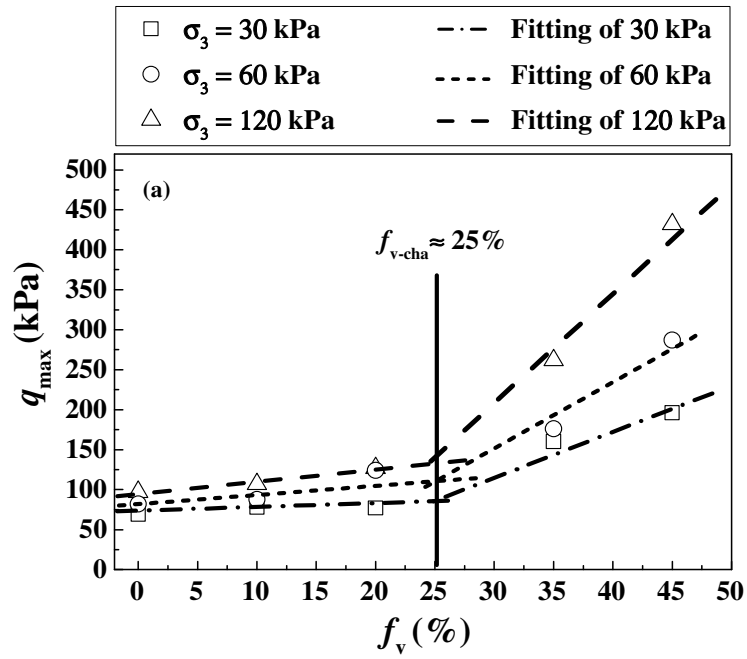
428

429

430



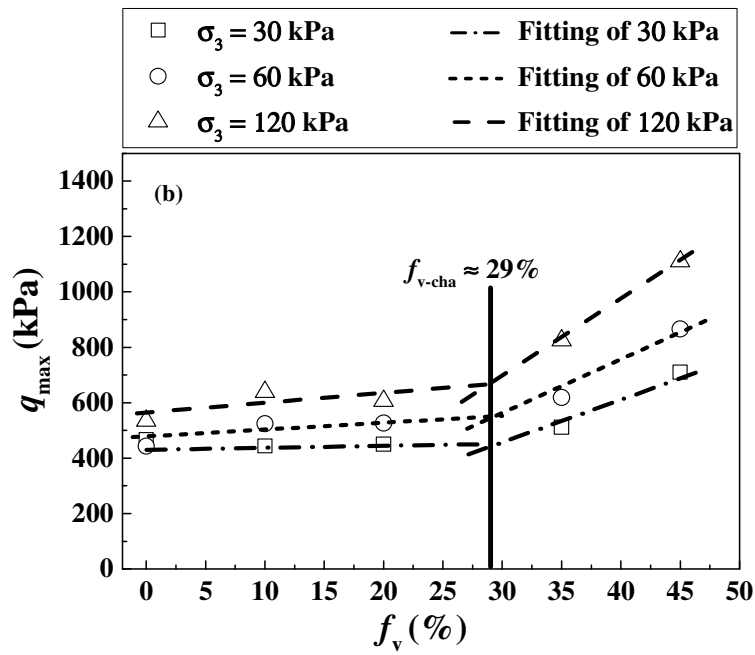
431



432

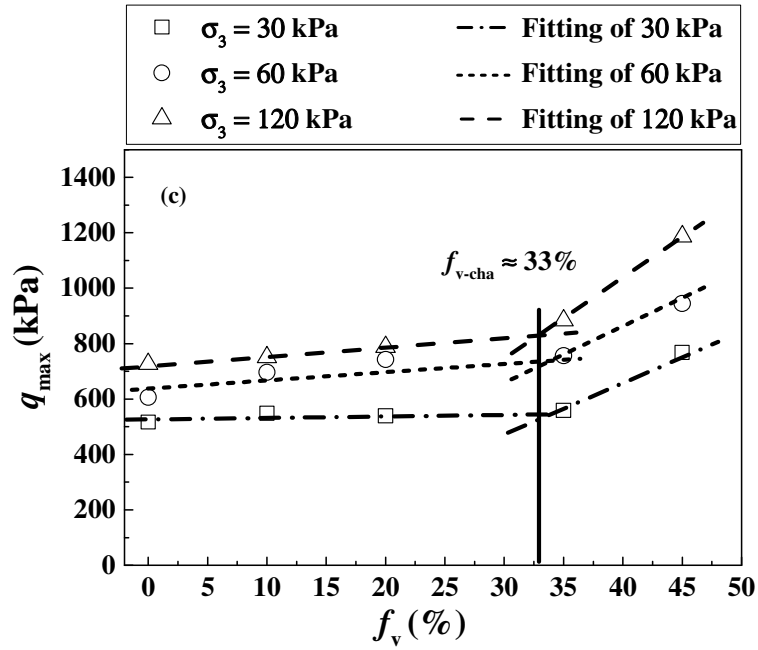
433

434



435

436



437

438

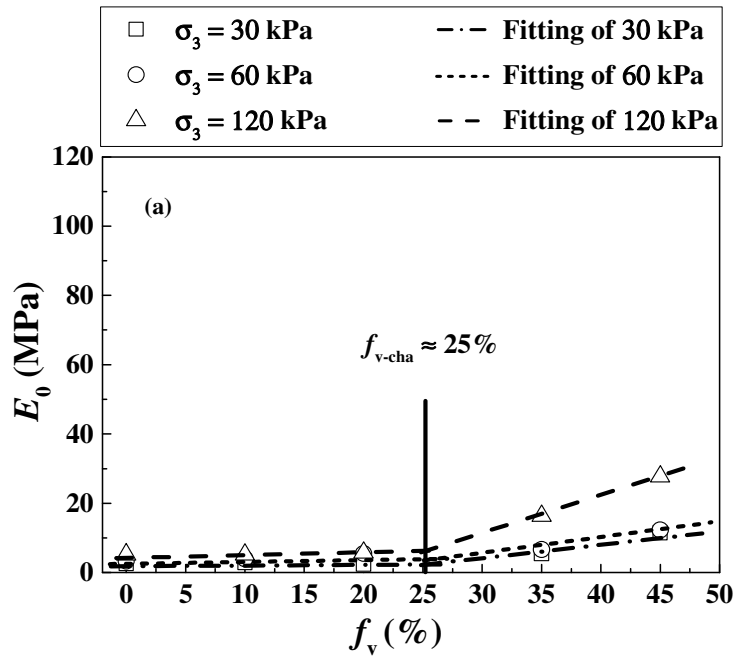
Fig. 7. Variations of peak deviator stress with  $f_v$  under different  $\sigma_3$  values for:

439

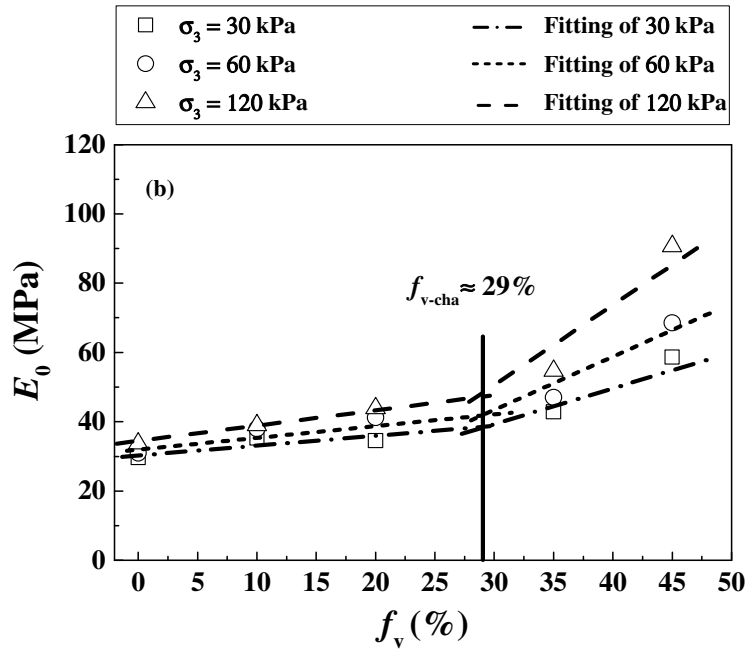
(a)  $w_1 = 17.6\%$ ; (b)  $w_2 = 10.6\%$ ; (c)  $w_3 = 7.0\%$

440

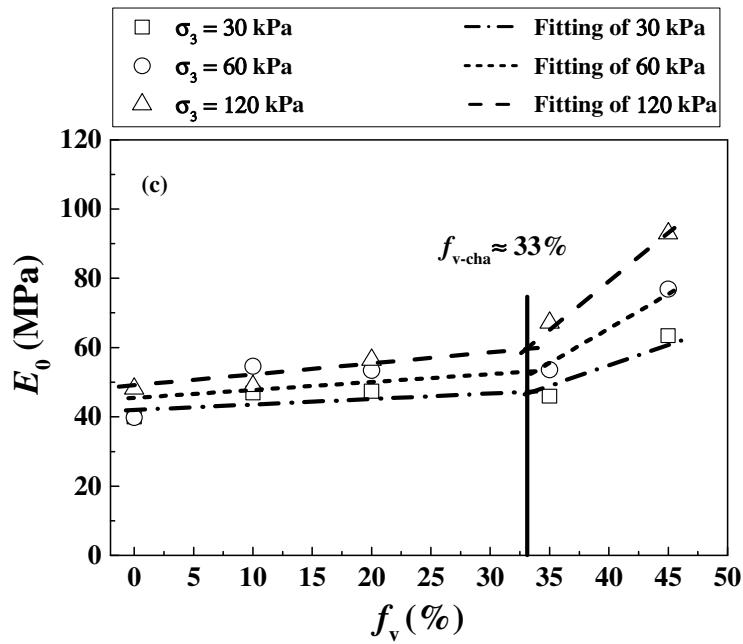
441



442



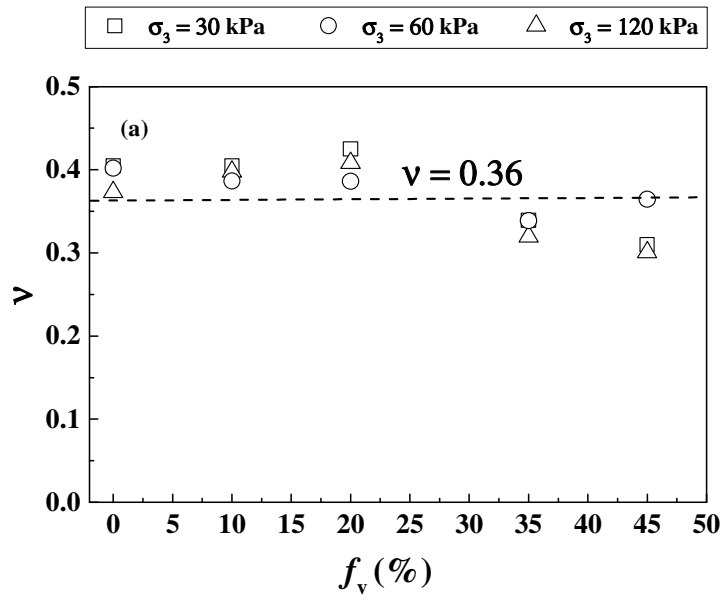
443  
444  
445



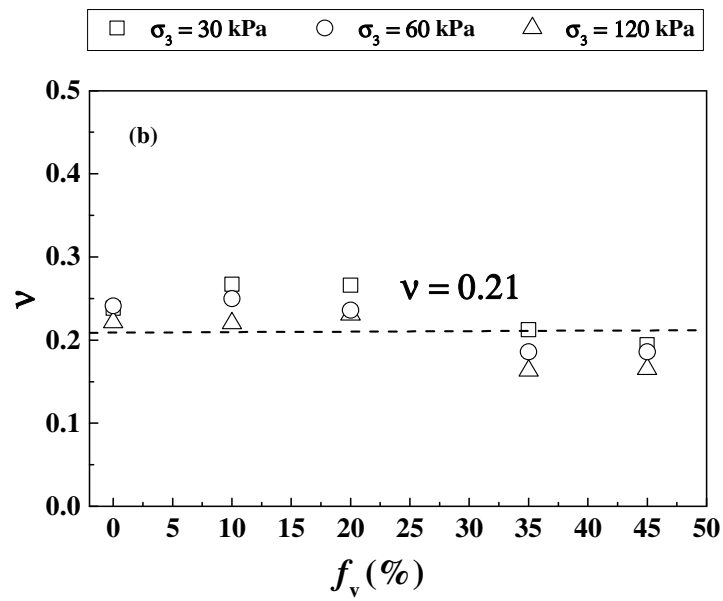
446  
447  
448  
449  
450  
451  
452

Fig. 8. Variations of initial Young's modulus with  $f_v$  under different  $\sigma_3$  values for:

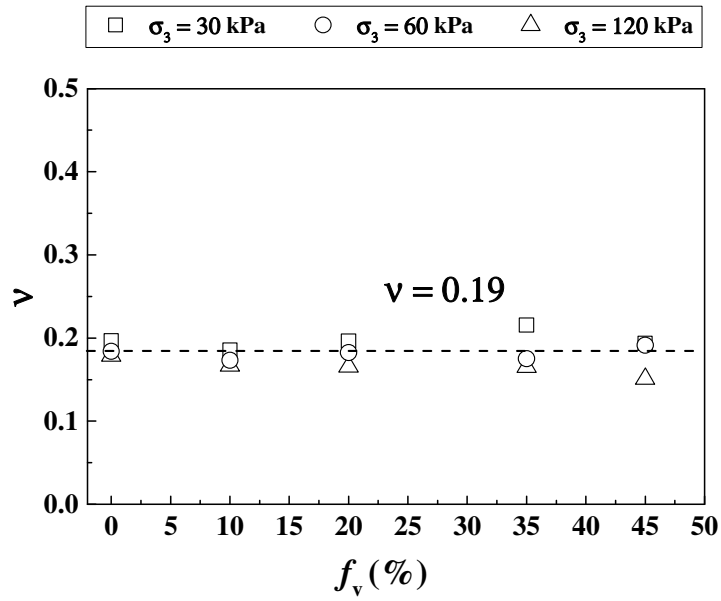
(a)  $w_1 = 17.6\%$ ; (b)  $w_2 = 10.6\%$ ; (c)  $w_3 = 7.0\%$



453



454



455

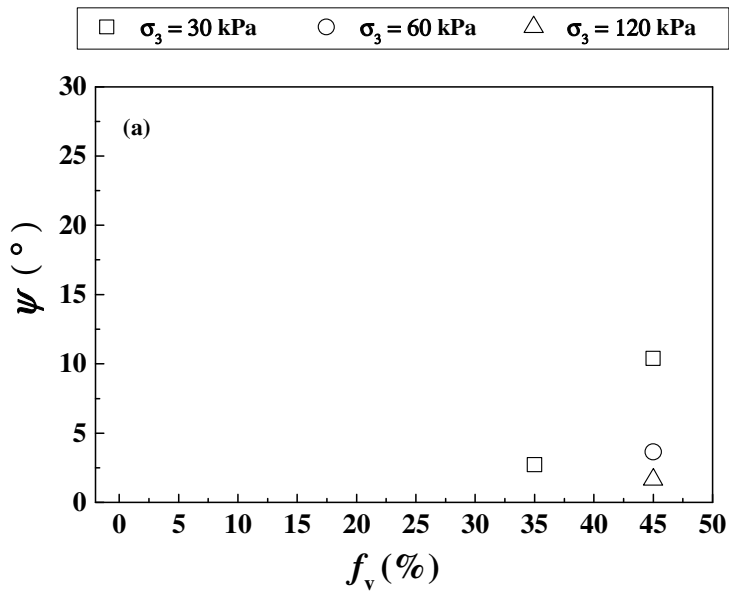
456

Fig. 9. Variations of Poisson's ratio with  $f_v$  under different  $\sigma_3$  values for:

457

(a)  $w_1 = 17.6\%$ ; (b)  $w_2 = 10.6\%$ ; (c)  $w_3 = 7.0\%$

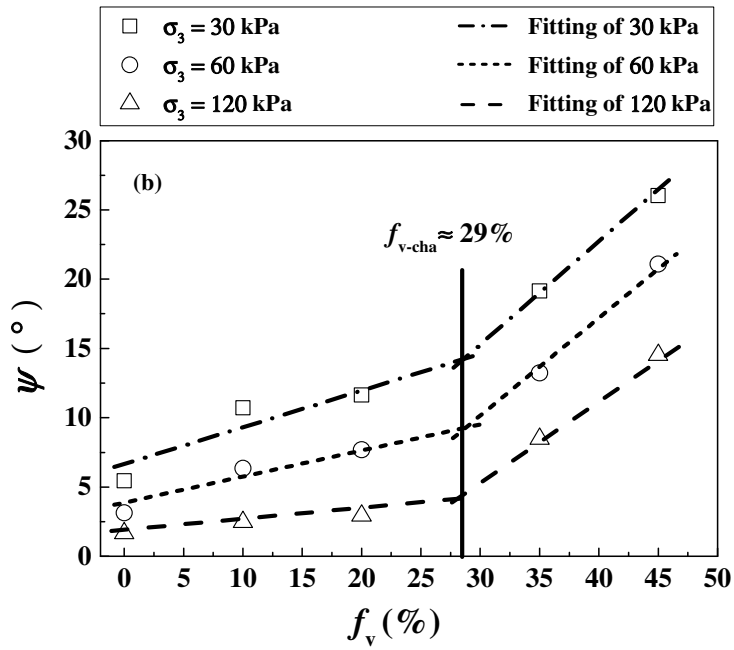
458



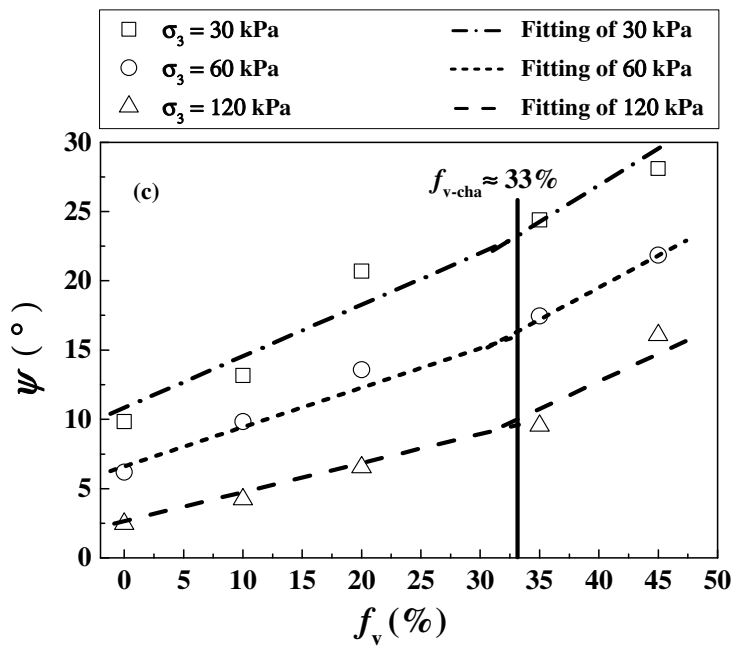
459

460

461



462



463

464

Fig. 10. Variations of dilatancy angle with  $f_v$  under different  $\sigma_3$  values for:

465

(a)  $w_1 = 17.6\%$ ; (b)  $w_2 = 10.6\%$ ; (c)  $w_3 = 7.0\%$

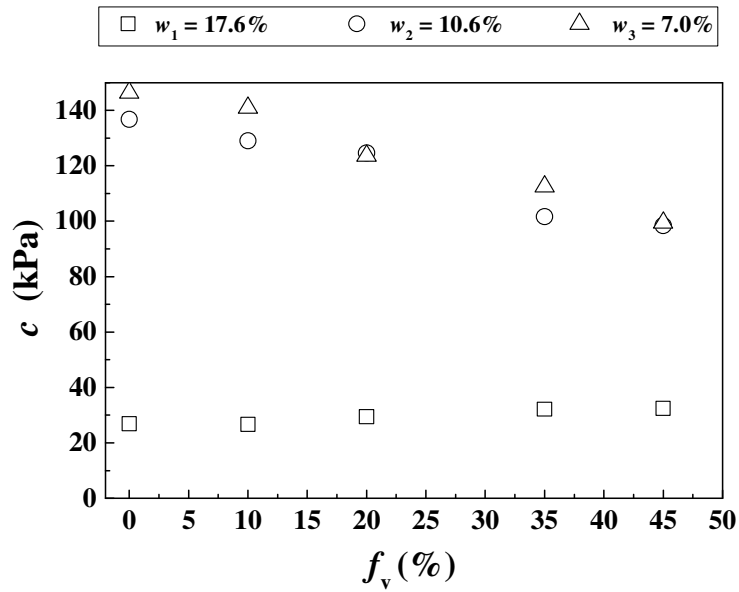
466

467

468

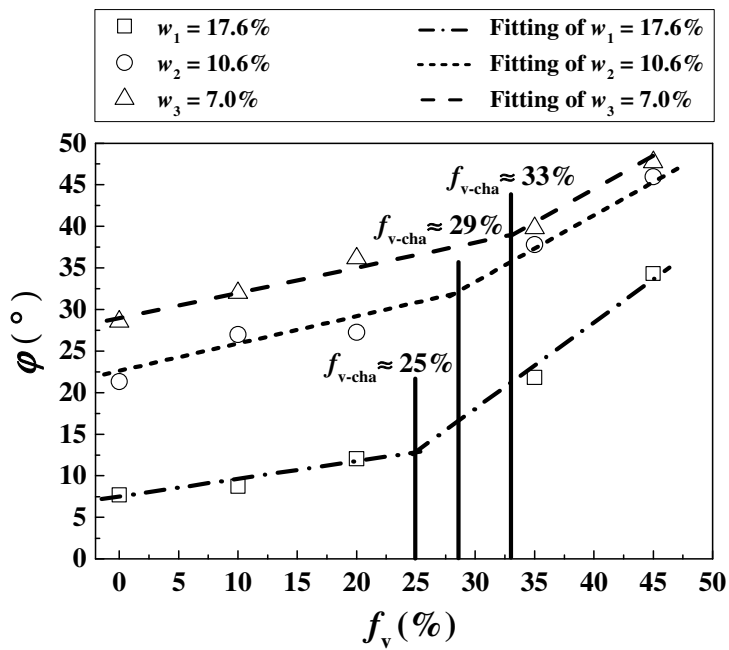
469

470



471  
472  
473  
474  
475

Fig. 11. Variations of cohesion with  $f_v$  under different water contents



476  
477  
478

Fig. 12. Variations of friction angle with  $f_v$  under different water contents